CRYSTAL GROWTH & DESIGN

pubs.acs.org/crystal

Article

Lattice Solvent-Directed Crystal Packing: Switching between Mer−Fac Isomerism and Spin Crossover in Fe(II) Complexes Based on 1,3,4-Thiadiazole

Jens-Georg Becker, Sriram Sundaresan, Luca M. Carrella, and Eva Rentschler*

Cite This: *Cryst. Growth Des.* 2026, 26, 4124−4132

Read Online

ACCESS | Metrics & More | Article Recommendations | Supporting Information

ABSTRACT: A direct correlation between solvent effects and coordination isomerism in iron(II) spin crossover complexes is reported using the novel ligand 1-(5-(naphthalen-2-yl)-1,3,4-thiadiazol-2-yl)-*N*,*N*-bis(pyridin-2-ylmethyl)methanamine ($L^{Naph\text{-}TDA}$). Crystallization from acetonitrile yields the facial isomer $[Fe(L^{Naph\text{-}TDA})(NCBH_3)_2]\cdot 2$ MeCN (**C1**), whereas a dichloromethane solution results in the meridional isomer $[Fe(L^{Naph\text{-}TDA})(NCBH_3)_2]\cdot 0.9$ DCM (**C2**). The two distinct coordination geometries were characterized by variable-temperature single-crystal X-ray diffraction, revealing solvent-dependent packing arrangements that modulate the SCO behavior. SQUID magnetometry shows that both solvatomorphs undergo spin transitions, and the differences in the dielectric properties of the lattice solvents likely contribute to the stabilization of the distinct isomers and the changes in observed cooperativity of the spin transition.

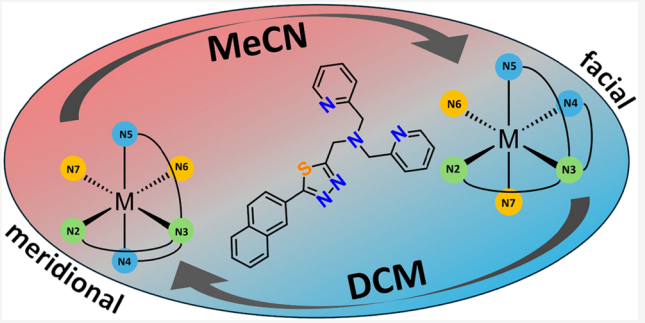

INTRODUCTION

Molecular bistability is central to functional molecular materials, enabling switchable responses to external stimuli such as temperature, light, or pressure.[1−4] Systems capable of switching between two distinct physical states are highly sought after for use in information storage, molecular logic gates, sensors, and actuators.[5−7] Among the various molecular switching motifs, spin crossover (SCO) compounds represent one of the most appealing classes, where a transition between low-spin (LS) and high-spin (HS) electronic configurations of a transition metal ion can be reversibly triggered by subtle changes in the environment.[8] This interplay between molecular structure, spin state, and collective solid-state effects continues to offer a fertile area of research, bridging coordination chemistry and crystal engineering.

A defining feature of SCO materials is their sensitivity to the crystal lattice environment.[9−11] Minute perturbations in molecular packing, hydrogen-bonding networks, or lattice solvation can dramatically alter the cooperative interactions responsible for the spin transition in the solid state.[12,13] Solvent molecules, in particular, often play a pivotal role in stabilizing distinct coordination geometries and governing the communication pathways between neighboring metal centers.[14,15] In some cases, the loss of this lattice solvent may lead to locking of the metal ions in one spin state.[16] Recent work by Nabeshima et al. demonstrates the reorganization of the coordination sphere between mer/fac-isomer in triply helical Fe(II) and Zn(II) complexes based on the solvent, but in all cases, the Fe(II) centers stayed in LS.[15] In this work, we report a rare example of 1,3,4-thiadizole based Fe(II) complex, where changes in the lattice solvent have aided in reorganizing the primary coordination sphere of the metal ion, leading to coordination isomerism between the *meridional* (mer) and *facial* (fac) forms.

Such solvent-driven geometric rearrangements are not just structural curiosities; they fundamentally reshape the ligand-field symmetry and, consequently, the spin-state energetics. The resulting reorganization of the crystal lattice modifies the packing density, symmetry relations, and magnetic cooperativity. This influences the spin states, which is a phenomenon that has been thoroughly investigated. This class of spin-crossover systems has potential applications as molecular sensors.

RESULTS AND DISCUSSION

Synthesis

The ligand 1-(5-(naphthalen-2-yl)-1,3,4-thiadiazol-2-yl)-*N*,*N*-bis(pyridin-2-ylmethyl)methanamine ($L^{Naph\text{-}TDA}$) was synthe-

Received: January 14, 2026
Revised: May 8, 2026
Accepted: May 11, 2026
Published: May 18, 2026

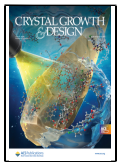

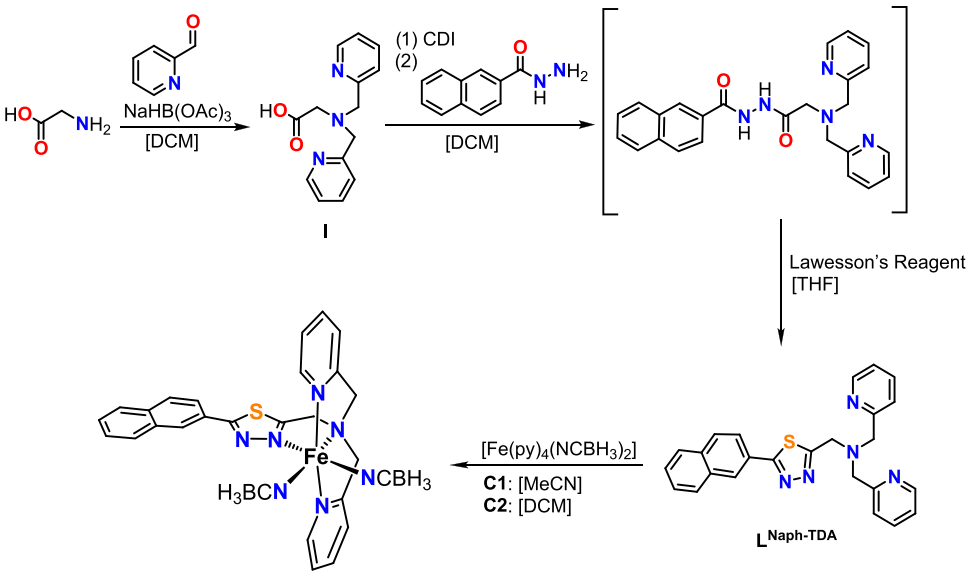

Figure 1. Multistep ligand synthesis of $L^{Naph\text{-}TDA}$, along with the complex synthesis of **C1** and **C2**.

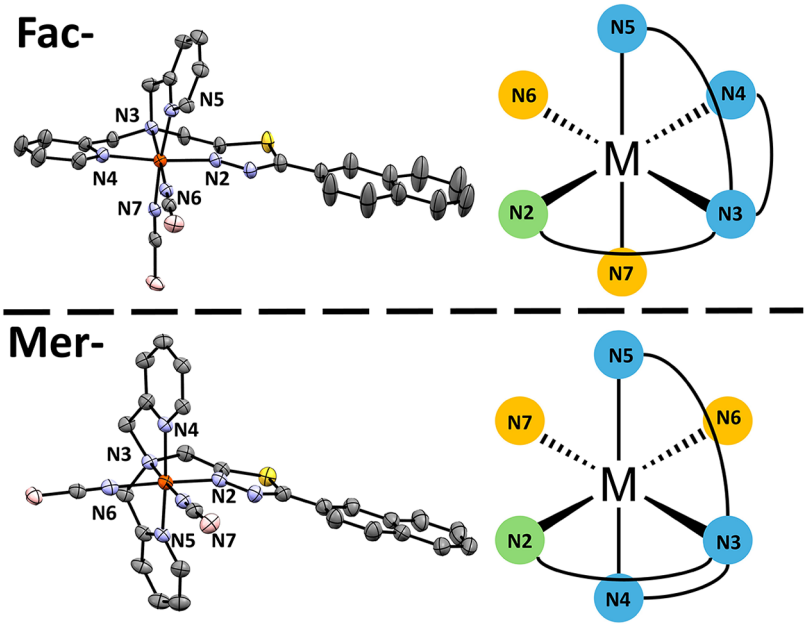

Figure 2. Difference in coordination mode between the fac-shaped $[Fe(L^{Naph\text{-}TDA})(NCBH_3)_2]\cdot 2$ MeCN (above) (**C1**) and the mer-shaped $[Fe(L^{Naph\text{-}TDA})(NCBH_3)_2]\cdot 0.9$ DCM (**C2**) (down) is shown by the molecular structure (left) at 120 K and schematically (right), with nitrogen atoms in **orange** for $NCBH_3$, **blue** for pyridine-units, bridging nitrogen and **green** for the 1,3,4-thiadiazole unit.

sized in two steps based on a previously reported procedure and is shown in Figure 1.[9] A modified synthesis procedure was used, using Lawesson's reagent to obtain the 1,3,4-thiadiazole instead of 1,3,4-oxadiazole, for which tetrabromomethane and triphenylphosphane are used.[9] The intermediate coupling product was obtained by reacting compound (**I**) with carbonyldiimidazole and naphthyl hydrazide in dry dichloromethane. After removing the solvent and dissolving the residue in tetrahydrofuran, cyclization and simultaneous substitution were achieved using Lawesson's reagent, yielding the desired product $L^{Naph\text{-}TDA}$ in moderate yield. A detailed description is provided in the experimental section. The newly obtained ligand was fully characterized using a range of techniques, including ^{1}H NMR, ^{13}C NMR, 2D NMR (Figures S3−S7), IR spectroscopy (Figure S8), mass spectrometry (Figures S11, S12), and elemental analysis.

$L^{Naph\text{-}TDA}$ was subsequently reacted with the well-known precursor $[Fe(NCBH_3)_2(py)_4]$ in two different solvents, acetonitrile (**C1**) and dichloromethane (**C2**).[17]

The complex synthesis in both cases was carried out under an inert atmosphere because of the air sensitivity of the complex precursor used. Both complexes **C1** and **C2** obtained are air-stable. Single crystals suitable for X-ray diffraction were obtained from both complexes in different crystallization conditions. In the case of **C1**, single crystals were obtained from the slow evaporation of acetonitrile, whereas in the case of **C2**, the layering method was used to obtain single crystals with dichloromethane and methanol.

https://doi.org/10.1021/acs.cgd.6c00054
Cryst. Growth Des. 2026, 26, 4124−4132

Both complexes were characterized by IR spectroscopy. A minor shift of the C=N stretching vibration within the aromatic ring was observed from 1586 cm^{-1} and 1567 cm^{-1} (free ligand) to 1603 cm^{-1} and 1571 cm^{-1} for **C1**, and to 1603 cm^{-1} and 1571 cm^{-1} for **C2** due to electron density changes upon coordination to iron(II). Additionally, the N≡C stretching vibration of the $NCBH_3$ coligand was observed at 2184 cm^{-1} (**C1**) and 2179 cm^{-1} (**C2**) (Figures S9 and S10).[9,17,18] Further confirmation of complex formation was provided by mass spectrometry, which revealed fragments such as $[Fe(L^{Naph\text{-}TDA})NC]^+$ (m/z: 505.089; 100%) (see Figures S13–S16). This is explained by the loss of one $NCBH_3$ coligand and by cleavage of the B–C bond, likely due to acidic conditions during the sample preparation or the measurement process.[19]

Elemental analysis (EA) confirmed solvent exchange in **C1**, from acetonitrile to water. In the case of **C2**, dichloromethane as a lattice solvent was verified by EA. Both were confirmed by infrared spectroscopy, as the **C1** sample used for further bulk analysis exhibited an O–H stretching vibration around 3000 cm^{-1}. Powder X-ray diffraction (XRD) (Figure S44) was used to verify the similarity between the measured single XRD structure and the microcrystalline sample used for the SQUID magnetometry.

Structural Determination

Single crystals of both complexes **C1** and **C2** crystallized in the same monoclinic crystal system. **C1** crystallized in the $P2_1/c$ space group with two acetonitrile molecules per complex unit, whereas **C2** crystallized in the $C2/c$ space group with 1.5 DCM per complex unit. The crystallography data are tabulated in Tables S1–S4.

Given that the different solvents led to different space groups, the influence on the molecular structure was further investigated. Complex **C1** exhibits a *fac*-isomer, characterized by the *cis*-coordination of the two pyridine rings among the four coordinating nitrogen atoms of the tetradentate ligand $L^{Naph\text{-}TDA}$, in addition to two $NCBH_3$ coligands (see Figure 2). On the other hand, complex **C2** shows the same N-donor coordination but with *trans*-coordinating pyridine units, leading to the *mer*-isomer, also illustrated in Figure 2.

The influence of the heteroatom on the bite angle and ligand flexibility was previously described by some of us as part of an investigation into the formation of helically chiral dinuclear complexes.[20] Since the reported complex also adopts the *mer*-configuration, this suggests that the presence of the 1,3,4-thiadiazole unit alone does not determine the coordination geometry. Instead, the introduction of the bulky naphthyl group in $L^{Naph\text{-}TDA}$ may contribute to a solvent-dependent isomerization through increased steric strain. These findings are also in line with literature reports from Kisslinger et al., who examined a series of complexes with comparable coordination motifs, varying the terminal N-donor functionalities.[21] The introduction of steric strain through substitution of the terminal amine with two methyl groups, or with bulkier groups such as propan-2-ylidene-imine and 1,1,3,3-tetramethylguanidine, showed that increasing strain favored *mer*-to-*fac* isomerization.[17] In another example by Matouzenko et al., the stereoisomerism of tetradentate ligands with a similar *motif* has been investigated in *fac*-$[Fe(DPPA)(NCS)_2]$ (DPPA = (3-aminopropyl)bis(2-pyridylmethyl)amine) and *mer*-$[Fe(DPEA)(NCS)_2]$ (DPEA = (3-aminoethyl)bis(2-pyridylmethyl)amine). In this study, elongation of the ligand's coordination arm led to a change in the coordination geometry from *fac* to *mer*.[22,23] However, in all cases described in the literature, the complexes are fixed in a specific spin state, either LS or HS. Therefore, the influence of the magnetic behavior associated with this structural rearrangement has never been investigated before. In our current example, however, the lattice solvent plays an active role in dictating the crystal packing, which in turn drives a *meridional-facial* reorientation, allowing for the first time to directly investigate the SCO response associated with such solvent-induced structural rearrangement.

The effect of deformation on the coordination sphere (C12–N2–Fe1–N3-C13) is illustrated by the observed out-of-plane distortions shown in Figure 3. The distortion was

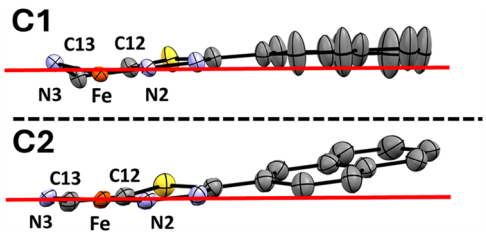

Figure 3. Out-of-plane distortion for the coordination pocket of the iron ion for the fac-shaped $[Fe(L^{Naph\text{-}TDA})(NCBH_3)_2]\cdot 2$ MeCN (above) (**C1**) and the mer-shaped $[Fe(L^{Naph\text{-}TDA})(NCBH_3)_2]\cdot 0.9$ DCM (**C2**) (down), with the calculated least-squares plane (red) based on the atoms in the coordination pocket (C12–N2–Fe1–N3-C13). The software Mercury was used to calculate the least-squares plane.

visualized through the calculation of the least-squares plane of the atoms in the coordination pocket (C12–N2–Fe1–N3-C13) using Mercury. The distortion is less pronounced for the mer-isomer (**C2**), with the atoms of the coordination sphere (C12–N2–Fe1–N3-C13) lying almost perfectly within the calculated plane. Conversely, the 1,3,4-thiadiazole-naphthyl unit of **C2** is significantly more curved, providing additional insight into the distortion caused by ligand strain.

The structural differences between complexes **C1** and **C2** were evaluated by comparing their distortion parameters (Tables S6 and S7). At 120 K, complex **C1** exhibits a distortion parameter $\sum_O(FeN_6)$ of 52.17°, which is significantly larger than that of **C2** and related complexes reported in the literature. The smaller value for **C2** ($\sum_O$ = 48.35°) is comparable to other reported *mer*-isomers such as $[Fe(L^{Ph\text{-}ODA})(NCBH_3)_2]\cdot MeCN$ ($\sum_O$ = 49.44°), $[Fe(L^{Ph\text{-}TDA})(NCBH_3)_2]\cdot H_2O$ ($\sum_O$ = 49.65°), and $[Fe(L^{Naph\text{-}ODA})(NCBH_3)_2]\cdot 1.5$ MeOH ($\sum_O$ = 47.04°), but lower than the chiral analogue $[Fe(L^{Naph\text{-}ODA\text{-}Al})(NCBH_3)_2]\cdot 0.5$ MeCN ($\sum_O$ = 57.94°).[9,17,24,25] This deviation is attributed to the steric influence of an introduced methyl group within the coordination sphere.[9] As all of these complexes are in the low-spin state at 120 K, the difference in distortion between the fac- and mer-isomers ($\Delta\sum_O$ = 3.82°) is considered significant. Given that both isomers share identical donor sets and ligand frameworks, this variation can be fully ascribed to their distinct coordination modes and first-sphere geometries.[26,27] Subtle modifications in the coordination environment, as reflected by the octahedral distortion parameter, are known to strongly influence spin crossover (SCO) behavior and critical temperatures.[28]

https://doi.org/10.1021/acs.cgd.6c00054
Cryst. Growth Des. 2026, 26, 4124–4132

The average Fe−N bond lengths for **C1** and **C2** are nearly identical (1.969 Å and 1.968 Å, respectively, Table S5), consistent with their low-spin configuration.[29] Upon transition to the high-spin state, an increase in Fe−N bond lengths and distortion parameters is expected due to the population of e_g* orbitals. This is true for **C1**, for which a marked increase in average bond length was observed at 230 K ($\bar{d}_{Fe-N}$ = 2.160 Å), indicating that the SCO occurs between 120 and 230 K. The increase is comparable to the high-spin analogues [Fe($L^{Ph\text{-}ODA}$)$(NCBH_3)_2$]·MeCN (2.174 Å), [Fe($L^{Ph\text{-}TDA}$)$(NCBH_3)_2$]·H_2O (2.15 Å) [Fe($L^{Naph\text{-}ODA}$)$(NCBH_3)_2$]·1.5 MeOH (2.165 Å), and [Fe($L^{Naph\text{-}ODA\text{-}Al}$)$(NCBH_3)_2$]·0.5 MeCN (2.162 Å).[9,17,24,25] Accordingly, the distortion parameter of **C1** increases substantially to $\sum_O$ = 102.76°, further confirming the spin state transition.[27]

In contrast, the Fe−N bond lengths for **C2** at 240 K remain relatively short ($\bar{d}_{Fe-N}$ = 2.034 Å), indicating that SCO is incomplete or only partially occurring. This is also reflected in a relatively low distortion parameter of $\sum_O$ = 65.35° at 240 K for **C2**, significantly below those of reported high-spin *mer*-isomers [Fe($L^{Ph\text{-}ODA}$)$(NCBH_3)_2$]·MeCN ($\sum_O$ = 97.26°), [Fe($L^{Ph\text{-}TDA}$)$(NCBH_3)_2$]·H_2O ($\sum_O$ = 86.90°), [Fe($L^{Naph\text{-}ODA}$)$(NCBH_3)_2$]·1.5 MeOH ($\sum_O$ = 92.92°) and [Fe($L^{Naph\text{-}ODA\text{-}Al}$)$(NCBH_3)_2$]·0.5 MeCN ($\sum_O$ = 89.78°), which are high-spin at 230 and 240 K, respectively.[9,17,24,25] The bond lengths of both complexes **C1** and **C2** at both measured temperatures are shown in Figure S43.

The space groups of **C1** and **C2** differ, suggesting that their intermolecular interactions must also be different. In particular, π−π stacking is known to affect the cooperativity and thus the abruptness of spin crossover. Since other factors, such as hydrogen bonding or solvent interactions, were not observed in the present crystal structures, which is supported by the apolar nature of the lattice solvents (DCM and MeCN), the discussion is limited to π−π interactions.[30]

In the crystal structure of both complexes, **C1** and **C2**, the complex fragment [Fe($L^{Naph\text{-}TDA}$)$(NCBH_3)_2$] occurs as pairs connected by the π−π-interaction of the naphthyl-1,3,4-thiadiazole-unit (shown in Figures S23, S30, S35, and S42). Based on the coordination isomer (*mer*/*fac*), the packing interactions differ between **C1** and **C2**, as detailed further below (Figures S22 and S37).[31,32] In the case of **C2**, the complexes form linear chains along the unit cell diagonal, stabilized by sequential naphthyl−naphthyl and pyridine−pyridine interactions (see Figure S37). This motive is in contrast to both reported 1,3,4-oxadiazole complexes [Fe($L^{Naph\text{-}ODA\text{-}Al}$)$(NCBH_3)_2$]·0.5 MeCN and [Fe($L^{Naph\text{-}ODA}$)$(NCBH_3)_2$]·1.5 MeOH, where the connection between the pairs occurs by interlocked iron(II) coordination pockets.[9,17] The stacking parameters for pyridine−pyridine interactions, calculated using the geometrical methods of B.K. Saha et al., are comparable across all systems and show minimal temperature dependence (Table S8, Figure S36).[33] The resulting chains of the complex pairs in the packing of **C2** are oriented along the *a*-*b*-face diagonal, while the next neighbor chain is turned by 45°. Solvent channels of dichloromethane are observed along the *c*-axis as the C−H bonds of the dichloromethane are oriented in the direction of the naphthyl group.

For **C1**, *fac*-coordination also facilitates naphthyl−naphthyl interactions but introduces additional interactions: thiadiazole−naphthyl and thiadiazole−pyridine stacking, which are oriented along the *a*-axis (Figures S21, S22, S24, and S25). These interactions result in a rectangular network along the *a*-axis, with solvent channels of acetonitrile along the *a*-direction (Figure S22). The additional interactions between the aromatic systems lead to a stronger network compared to **C2**, which affects the spin state profile, resulting in a higher degree of cooperativity and, consequently, a more abrupt profile. The stacking parameters suggest that the naphthyl−naphthyl interactions in **C1** are stronger, as indicated by a 1.3 Å smaller offset compared to **C2** (Table S8). The interaction strength is also reflected in the unit cell expansion observed upon heating. A modest unit cell volume increase by 2% is observed for **C1** and by 4% for **C2**. These expansions are relatively small when compared to the 9% volume change reported for the oxygen analogue [Fe($L^{Naph\text{-}ODA}$) $(NCBH_3)_2$]·3 MeOH.[17]

Notably, the naphthyl−naphthyl interactions in **C1** undergo a decrease in offset upon heating, coupled with a rotation around the 1,3,4-thiadiazole-naphthyl bond (shown in Figure 4). This is quantified by a change in the torsion angle C1−C10−C11−N1 (with C10−C11 being the bond between the naphthyl and thiadiazole units), which shifts by approximately 22°. This rotational flexibility may significantly influence the cooperative behavior of spin transition.

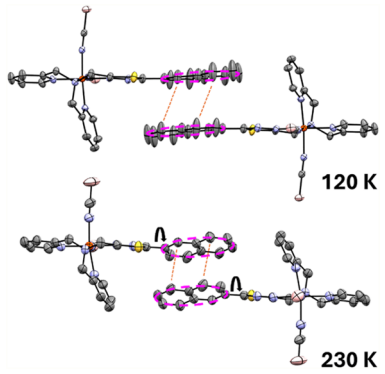

Figure 4. Naphthyl−naphthyl-rotation observed by VT single-crystal XRD for the fac-shaped complex [Fe($L^{Naph\text{-}TDA}$)$(NCBH_3)_2$]·2 MeCN (**C1**) at 120 K (above) and 230 K (bottom).

A similar study was demonstrated by Zhao et al. for the enantiopure complex [(R-L)Fe{$Au(CN)_2$}$_2$] (R-L = (R)-N^1-N^2-dibenzyl-N^1-N^2-bis(pyridine-2-ylmethyl)propan-1,2-diamine), where a symmetry-breaking transition due to the spring-like motion of benzyl rings enabled hysteresis in the magnetic response.[34] In their study, motion of the benzylic groups between 280 and 380 K led to a two-step spin transition, including a symmetry change from $P2_12_12_1$ to $P2_1$ and a spin transition from high-spin to low-spin states, demonstrating the profound impact of intramolecular flexibility on SCO hysteresis.

Solid State Magnetism

To investigate the influence of the coordination isomer in the solid state, magnetic measurements were performed on microcrystalline powder using a SQUID magnetometer. These measurements were performed upon cooling from 300 to 10 K and heating from 10 to 300 K, at an effective scan rate of 2.5 K/min, for both complexes in settle mode (see Figure 5). For **C1**, SQUID measurements were performed on the solvated sample (suggesting [Fe($L^{Naph\text{-}TDA}$)$(NCBH_3)_2$]·2 MeCN) using the mother liquor. To demonstrate the impact

https://doi.org/10.1021/acs.cgd.6c00054
Cryst. Growth Des. 2026, 26, 4124−4132

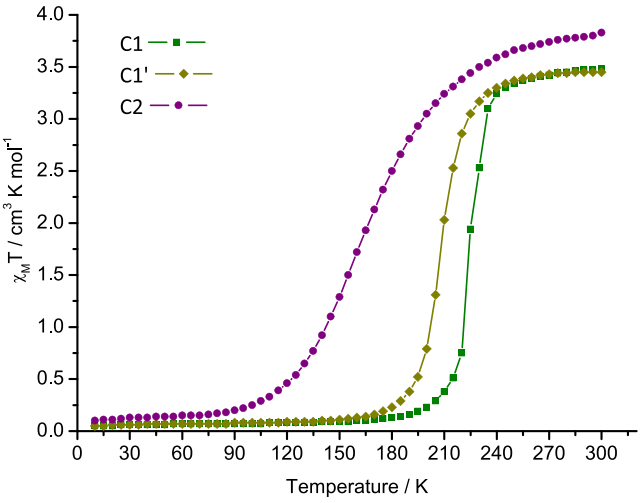

Figure 5. χ_MT vs T of [Fe($\mathbf{L}^{\text{Naph-TDA}}$)$(NCBH_3)_2$]·2 MeCN (**C1**) with the mother liquor (green), the same sample after exposure to humidity and lattice solvent exchange (yellow) and [Fe($\mathbf{L}^{\text{Naph-TDA}}$)-$(NCBH_3)_2$]·0.9 DCM (**C2**) (purple) from 300 to 10 K.

of the lattice solvent, the sample was exposed to humidity, after which the lattice solvent acetonitrile was exchanged with water, verified by elemental analysis (see Figure S46).

Both complexes reach a χ_MT value of approximately 3.5 cm^3·K·mol^{-1} at high temperatures, which is characteristic of the T_{2g} high-spin state of Fe(II). A clear plateau is seen in the case of **C1**.[35] Upon cooling, complex **C2** displays a gradual decrease in χ_MT between 250 and 100 K, with a critical temperature of $T_C^{\uparrow}$ = $T_C^{\downarrow}$ = 165 K. The χ_MT value reaches a low-temperature plateau of 0.09 cm^3·K·mol^{-1}, consistent with conversion to the A_{1g} low-spin state via spin crossover.[35]

At room temperature, the χ_MT value for **C1** is 3.47 cm^3·K·mol^{-1}, consistent with values reported for high-spin iron(II) complexes with comparable coordination geometry.[17] Upon cooling, the χ_MT value decreases abruptly between 240 and 210 K, reaching 0.38 cm^3·K·mol^{-1}. This is followed by a gradual decrease to a low-spin plateau of 0.05 cm^3·K·mol^{-1}, indicative of complete conversion to the A_{1g} low-spin state. The critical temperature (T_C) during cooling was determined as the temperature at which 50% of the χ_MT of the fully high-spin state is reached, yielding T_C = 225 K. Exchanging acetonitrile for water as lattice solvent results in a change in the spin crossover profile (see Figure S46). It is known that the lattice solvent has an impact on the cooperativity and transition temperatures.[36] At high temperatures, a plateau is observed with χ_MT values (3.45 cm^3·K·mol^{-1}) similar to those of the solvated sample. Upon cooling, a shift in the critical temperature is observed, decreasing to T_C = 207 K. Powder XRD confirms that the SQUID sample of **C1** corresponds to the crystal structure. This indicates that the rotation of the naphthyl groups does not significantly influence the spin crossover temperature, as might be expected based on the literature.[34]

Further, by correlating the packing effects to the magnetic behavior, we observe, in the packing of **C1**, that the additional interactions between the aromatic groups are leading to a stronger network compared to **C2**. This is reflected in the abrupt spin state transition observed for **C1**, in contrast to the more gradual spin transition by **C2**, where weaker interactions between the complex units exist. The distinct coordination geometries observed for the two complexes originate from the nature of the lattice solvent, which acts as a key structure-directing factor during crystallization. Although both species are derived from the same molecular components and exhibit $\pi-\pi$ stacking interactions between the naphthyl groups, crystallization from different solvents stabilizes different coordination isomers, namely, the facial (**C1**) and meridional (**C2**) forms. This solvent-dependent isomer selection leads to a change in the relative orientation of one pyridyl donor with respect to the 1,3,4-thiadiazole unit, being *trans* in **C1** and *cis* in **C2.**

As a consequence, the two isomers display markedly different supramolecular interaction patterns. In the facial isomer, the lower symmetry enables a higher degree of intermolecular connectivity, where the pyridyl group trans to the thiadiazole unit engages in additional $\pi-\pi$ interactions with the thiadiazole ring of a neighboring molecule, giving rise to an extended interaction network. In contrast, the meridional isomer lacks such cross-interactions and is instead characterized by comparatively weaker pyridine−pyridine contacts.

Thus, the lattice solvent not only governs the coordination geometry but also dictates the resulting crystal packing and intermolecular interactions. These differences directly influence the degree of cooperativity within the lattice, ultimately leading to the distinct spin-crossover behaviors observed for the two complexes. The lattice solvent is well-known to influence the profile of the spin crossover, due to intermolecular interactions.[37,38]

The two solvatomorphs of the 1,3,4-thiadiazole-based Fe(II) complex display distinct coordination modes and spin-crossover behaviors, reflecting the combined influence of lattice polarity and coordination geometry. In **C1** ($\varepsilon \approx 36$ (MeCN as in XRD) and 80 (H_2O as in bulk sample by EA)), a facial (fac) arrangement of the FeN_6 core is stabilized, resulting in a more symmetric ligand field and shorter average Fe−N distances. The parameter ε denotes the dielectric constant of the lattice solvent. This is consistent with a dominant low-spin character and a higher $T_{1/2}$. The observed framework of $\pi-\pi$ interactions results in a higher degree of cooperativity.[39] In contrast, the dichloromethane solvate ($\varepsilon \approx 9$) favors a meridional (mer) configuration, introducing greater angular distortion and a weaker ligand field, correlating with the predominance of the high-spin state.[39] These observations suggest that the dielectric nature of the lattice solvent exerts an indirect yet significant impact: the more polar lattice enhances electrostatic screening and intermolecular coupling, thereby stabilizing the low-spin configuration. In contrast, the less polar DCM lattice weakens these interactions and promotes high-spin behavior. Further evidence on solvent polarity-dependent coordination isomers was presented by Nabeshima et al. through the analysis of the equilibrium between *fac* and *mer*-coordination in *tris* coordinated helical motif of iron(II) in various solvents using solution NMR.[15] This solvent-driven reorganization of coordination geometry and spin state exemplifies how lattice polarity and local structure cooperatively govern the electronic bistability in SCO materials.

CONCLUSION

In conclusion, we report the synthesis and detailed characterization of the novel ligand 1-(5-(naphthalen-2-yl)-1,3,4-thiadiazol-2-yl)-*N*,*N*-bis(pyridin-2-ylmethyl)methanamine ($\mathbf{L}^{\text{Naph-TDA}}$) and two solvatomorph complexes, **C1** [Fe($\mathbf{L}^{\text{Naph-TDA}}$)$(NCBH_3)_2$]·2 MeCN and **C2** [Fe($\mathbf{L}^{\text{Naph-TDA}}$)-

https://doi.org/10.1021/acs.cgd.6c00054
Cryst. Growth Des. 2026, 26, 4124−4132

$(NCBH_3)_2]\cdot 0.9$ DCM. The crystallization solvent exerts a decisive influence on the coordination geometry, with acetonitrile favoring formation of the facial isomer, whereas dichloromethane stabilizes the meridional isomer, highlighting a pronounced solvent-dependent isomerization effect. Variable-temperature SQUID magnetometry reveals a shift in the SCO behavior between the two solvatomorphs, which can be directly correlated with their coordination mode and the distinct packing arrangements, as elucidated by single-crystal X-ray diffraction. The fac- and mer-isomers exhibit fundamentally different packing motifs, leading to pronounced differences in both the SCO temperature and the cooperativity of the transition.

This work highlights that solvent choice not only determines the coordination isomer formed but, through the resulting packing arrangement, also governs the magnetic response of the material. In particular, the dielectric character of the incorporated solvent plays a critical role in modulating the intermolecular interactions within the crystal lattice. These findings establish solvent selection as a powerful and predictive strategy for controlling coordination isomerism and fine-tuning the SCO properties in iron(II) systems. Ongoing studies aim to further elucidate the relationship between coordination isomerism and other facets of ligand design.

EXPERIMENTAL SECTION

All chemicals were purchased from Alfa Aesar, Deutero, Fisher Chemicals, TCI, Sigma-Aldrich, and Acros Organics and were used without further purification. Solvents were dried according to the literature-known procedures and used freshly distilled.[40] NMR spectra were recorded at room temperature with a Bruker Avance DSX 400 and analyzed with the program MestReNova.[41] Magnetic susceptibility measurements were performed on a Quantum Design SQUID magnetometer MPMS3-EC in a temperature range between 10 and 300 K with an applied field of 1 kOe. All mass spectra (Advion expression-L CMS) as well as elemental analysis (Elementar vario EL Cube: C, H, and N) were measured at the microanalytical laboratories of the Johannes Gutenberg University Mainz. X-ray diffraction data were collected with an STOE STADIVARI instrument at the Johannes Gutenberg University Mainz. The structures were solved with ShelXT[42] and refined with ShelXL[43,44] implemented in the program Olex2.[45] The X-ray cif file data are deposited on the Cambridge CCDC database with identification numbers 2501268–2501271. UV–vis absorption spectroscopy was performed using the JASCO V-770 in a single-beam mode with a scanning speed of 400 nm/min. The data were plotted using Origin 7.5 V5. The ATR-IR spectra were recorded at room temperature on a Bruker ALPHA II ATR-IR, analyzed with the software OPUS and plotted in Origin 7.5 V5. The conductivity measurements were performed for the samples in acetonitrile using a *SevenCompactTM S230* conductivity meter. The arithmetic mean of three measurements was used for the calculation of the molar conductivity.

LIGAND SYNTHESIS

The synthesis of 1-(5-(naphthalen-2-yl)-1,3,4-thiadiazol-2-yl)-*N*,*N*-bis(pyridin-2-ylmethyl)methanamine of $\mathbf{L}^{\mathbf{Naph\text{-}TDA}}$ was done similar to the reported.[9]

2-Naphthohydrazide

2-Naphthohydrazide was prepared based on the previously reported literature.[17,46] Naphthoic acid (20.00 g, 116.20 mmol, 1.0 equiv) was dissolved in 300 mL of ethanol, and sulfuric acid (4 mL, conc.) was added. The solution was refluxed over 24 h at 90 °C. The solvent was removed under reduced pressure, and the residue was dissolved in 300 mL of dichloromethane. The organic phase was washed three times with 100 mL of sodium bicarbonate (5%), the organic phase was dried over magnesium sulfate, and the solution was concentrated under reduced pressure. The residue was dissolved in 100 mL of methanol, and hydrazine hydrate (6.31 mL, 127.80 mmol, 1.1 equiv) was added to the solution, which was then refluxed for over 24 h at 75 °C. While cooling down the solution, a beige solid was obtained and separated by filtration. The resulted beige solid was washed three times with 30 mL of cold methanol and with 30 mL of *n*-pentane to yield 2-naphthohydrazide (18.60 g, 99.89 mmol, 86%). ^{1}H NMR (400 MHz, DMSO-d_6 δ(ppm)) 9.96 (s, 1H), 8.44 (d, J = 1.7 Hz, 1H), 8.04–7.89 (m, 5H), 7.65–7.54 (m, 2H), 4.61 (s, 2H).

Bis(Pyridine-2-yl)glycine (I)

The synthesis procedure of bis(pyridine-2-yl)glycine (**I**) was reported by Levadala et al.[47]

Glycine (3.00 g, 79.93 mmol, 1.0 equiv) was suspended in 80 mL of dichloromethane under a nitrogen atmosphere. Under cooling with ice, sodium triacetoxyborohydride (21.18 g, 99.91 mmol, 2.5 equiv) was added and stirred. After 10 min, a solution of 2-pyridinecarbaldehyde (7.60 mL, 79.93 mmol, 2.0 equiv) in 20 mL of dichloromethane was added. The cooling was replaced, and the yellowish suspension was allowed to warm up overnight. 70 mL of saturated sodium bicarbonate solution was added. After 30 min, the two phases were extracted, and the aqueous phase was extracted twice with 150 mL of dichloromethane. The organic phase was dried over sodium sulfate, and the solvent was removed under reduced pressure. The crude product was purified via column chromatography (dichloromethane:methanol; 90:10). The product was isolated as brown powder (3.113 g, 12.10 mmol, 30%).^{1}H NMR (400 MHz, chloroform-d δ(ppm)): 8.59–8.53 (m, 2H), 7.67 (td, J = 7.7, 1.8 Hz, 1H), 7.33–7.29 (m, 1H), 7.23 (ddd, J = 7.6, 4.9, 1.2 Hz, 1H), 4.11 (s, 2H), 3.61 (s, 1H).

1-(5-(Naphthalen-2-yl)-1,3,4-thiadiazol-2-yl)-*N*,*N*-bis(pyridin-2-ylmethyl)methanamine ($\mathbf{L}^{\mathbf{Naph\text{-}TDA}}$). Bis(pyridin-2-ylmethyl)glycine (**I**) (5.260 g, 20.44 mmol, 1 equiv) was dissolved under a nitrogen atmosphere in dry dichloromethane, and the solution was cooled with ice. Carbonyldiimidazole (3.708 g, 22.87 mmol, 1.1 equiv) was added, and the clear solution was stirred under cooling for 30 min. Naphthohydrazide (3.807 g, 20.44 mmol, 1 equiv) was added, and the suspension was allowed to warm up and stirred overnight. Then, the solvent was evaporated under vacuum, and the residue was dissolved in dry tetrahydrofuran under a nitrogen atmosphere. To the clear brown solution, Lawesson's reagent (9.907 g, 24.53 mmol, 1.2 equiv) was added, and the resulting reddish-brown solution was heated under reflux at 80 °C overnight. Then, the solvent was removed under vacuum, and the residue was dissolved in 400 mL of dichloromethane. The organic phase was washed three times with saturated sodium bicarbonate solution and dried over sodium sulfate. The desired product 1-(5-(naphthalen-2-yl)-1,3,4-thiadiazol-2-yl)-*N*,*N*-bis(pyridin-2-ylmethyl)methanamine ($\mathbf{L}^{\mathbf{Naph\text{-}TDA}}$) (3.566 g, 8.43 mmol, 41%) was obtained after purification with flash chromatography of the vacuum concentrated organic phase as a brown solid in moderate yields. ^{1}H NMR (400 MHz, chloroform-*d* δ(ppm)): 8.59 (ddd, J = 4.9, 1.8, 0.9 Hz, 2*H*), 8.42 (d, J = 1.8 Hz, 1*H*), 8.12 (dd, J = 8.6, 1.8 Hz, 1*H*), 7.97–7.85 (m, 3*H*), 7.73 (td, J = 7.7, 1.8 Hz, 2*H*), 7.60 (dt, J = 7.9, 1.1 Hz, 2*H*), 7.58–7.53 (m, 2*H*), 7.21 (ddd, J = 7.5, 4.9,

https://doi.org/10.1021/acs.cgd.6c00054
Cryst. Growth Des. 2026, 26, 4124–4132

1.2 Hz, 2H), 4.25 (s, 2H), 4.00 (s, 4H). ^{13}C NMR (101 MHz, $CDCl_3$, δ (ppm)): 158, 149, 137, 134, 133, 129, 128, 1278, 128 (d, J = 10.3 Hz), 127, 124, 123, 122, 59, 53. FT-IR: $\tilde{\nu}$ (cm^{-1}) = 3045, 3009, 2960, 2929, 2880, 2837, 1680, 1586, 1567, 1510, 1473, 1431, 1416, 1347, 1321, 1302, 1283, 1242, 1216, 1192, 1175, 1147, 1131, 1112, 1071, 1047, 992, 977, 937, 908, 871, 857, 842, 813, 770, 760, 743, 680, 653, 629, 606, 585, 565, 519, 481, 405. ESI-MS (m/z): calc. for $[C_{25}H_{21}N_5S_1]^+$ expected: 424.159 (100.00%); found: 424.160 (100.00%). Elemental analysis calculated for $\mathbf{L}^{\mathbf{Naph\text{-}TDA}}$ 0.5 H_2O (C_{25} H_{26} $N_5O_{0.5}S$): C, 63.71; H, 4.08; N, 16.36. Found: C, 69.70; H, 4.81; N, 15,90.

COMPLEX SYNTHESIS

The $[Fe(py)_4(NCBH_3)_2]$ precursor was prepared according to the literature.[48]

$[Fe(L^{Naph\text{-}TDA})(NCBH_3)_2]$·2 MeCN (C1)

The following reaction was carried out in a glovebox under an inert atmosphere. $[Fe(py)_4(NCBH_3)_2]$ (109 mg, 0.24 mmol, 1 equiv) was dissolved in acetonitrile (8 mL) and stirred for 30 min. The solution was filtered with a syringe filter to remove undissolved particles. The filtrate was added to a solution of 1-(5-(naphthalen-2-yl)-1,3,4-thiadiazol-2-yl)-*N*,*N*-bis(pyridin-2-ylmethyl)methanamine ($\mathbf{L}^{\mathbf{Naph\text{-}TDA}}$) (100 mg, 0.24 mmol, 1 equiv) in 1 mL of acetonitrile. The solution was stirred for 30 min again and filtered into an empty vial using a syringe filter. The solution was kept undisturbed and set for slow evaporation of the solvent. After 4 days, brown block-shaped crystals had formed that were suitable for X-ray structure analysis. The crystals were collected by filtration and dried at atmospheric pressure to afford $[Fe(\mathbf{L}^{\mathbf{Naph\text{-}TDA}})(NCBH_3)_2]$·2 MeCN (101.00 mg, 0.181 mmol, 77%) at high yields. FT-IR: $\tilde{\nu}$ (cm^{-1}) = 3053, 2336, 2184, 1603, 1571, 1479, 1439, 1369, 1356, 1319, 1289, 1266, 1191, 1191, 1191, 1156, 1117, 1096, 1054, 1054, 1017, 995, 976, 958, 938, 897, 884, 863, 820, 796, 767, 752, 704, 652, 615, 560, 513, 475, 425, 410. ESI-MS (m/z): calc. for $[C_{26}H_{21}FeN_6S]^+$ expected: 505.089 (100.00%); found: 505.089 (100.00%). Elemental analysis calculated for $[Fe(\mathbf{L}^{\mathbf{Naph\text{-}TDA}})(NCBH_3)_2]$·0.5 H_2O ($C_{27}H_{28}N_7B_2FeO_{0.5}S$): C, 57.09; H, 4.97; N, 17.26. Found: C, 56.72; H, 5.09; N, 17.16. Since the EA was not measured immediately after isolation from the mother liquor, the lattice solvent MeCN is replaced by water.

$[Fe(L^{Naph\text{-}TDA})(NCBH_3)_2]$·0.9 DCM (C2)

The following reaction was carried out in a glovebox under an inert atmosphere. $[Fe(py)_4(NCBH_3)_2]$ (109 mg, 0.24 mmol, 1 equiv) was dissolved in 5 mL of dry methanol and stirred for 30 min, resulting in a red solution. The solution was filtered using a syringe filter to remove undissolved particles. The filtrate was layered above a spacer solution of 1:1 dichloromethane and methanol, which was layered on a solution of 1-(5-(naphthalen-2-yl)-1,3,4-thiadiazol-2-yl)-*N*,*N*-bis(pyridin-2-ylmethyl)methanamine ($\mathbf{L}^{\mathbf{Naph\text{-}TDA}}$) (100 mg, 0.24 mmol, 1 equiv) in 5 mL of dichloromethane. Crystals suitable for X-ray structure analysis were obtained after 6 days out of the reddish solution. The crystals were collected by filtration, dried at atmospheric pressure to afford $[Fe(\mathbf{L}^{\mathbf{Naph\text{-}TDA}})(NCBH_3)_2]$ · 0.9 DCM (65.00 mg, 0.107 mmol, 45%). FT-IR: $\tilde{\nu}$ (cm^{-1}) = 2916, 2337, 2179, 1603, 1571, 1478, 1440, 1349, 1305, 1283, 1217, 1192, 1155, 1110, 1049, 1019, 996, 956, 938, 897, 862, 821, 789, 758, 731, 705, 657, 642, 473, 421. ESI-MS (m/z): calc. for $[C_{26}H_{21}FeN_6S]^+$ expected: 505,089 (100.00%); found: 505.089 (100.00%). Elemental analysis calculated for $[Fe(\mathbf{L}^{\mathbf{Naph\text{-}TDA}})(NCBH_3)_2]$ · 0.9 CH_2Cl_2 ($C_{28}H_{28.8}N_7B_2FeSCl_{1.8}$): C, 52.73; H, 4.57; N, 15.43. Found: C, 52.53; H, 4.73; N, 15.62. The EA was measured immediately after isolation from the mother liquor

ASSOCIATED CONTENT

Data Availability Statement

All of the processed data are presented in the main manuscript and the ESI. The crystallography data collected are deposited in the Cambridge crystal structure database with the identification numbers 2501268−2501271. All of the raw data from this manuscript have been uploaded to Zenodo and are freely available via the DOI: 10.5281/zenodo.17609619.

Supporting Information

The Supporting Information is available free of charge at https://pubs.acs.org/doi/10.1021/acs.cgd.6c00054.

^{1}H, ^{13}C, COSY, HMBC, and HSQC spectra of the ligand; IR spectra of the ligand and complexes; HRes-ESI mass spectra of ligand and complexes; crystallographic data containing bond length tables and bond angles; crystal structures; packing pictures; magnetic susceptibility measurements; and UV−vis spectra of the ligand and complexes (PDF)

Accession Codes

Deposition Numbers 2501268−2501271 contain the supplementary crystallographic data for this paper. These data can be obtained free of charge via the joint Cambridge Crystallographic Data Center (CCDC) and Fachinformationszentrum Karlsruhe Access Structures service.

AUTHOR INFORMATION

Corresponding Author

Eva Rentschler − *Department Chemie, Johannes Gutenberg-Universität Mainz, 55128 Mainz, Germany;* orcid.org/0000-0003-1431-3641; Email: rentschl@uni-mainz.de

Authors

Jens-Georg Becker − *Department Chemie, Johannes Gutenberg-Universität Mainz, 55128 Mainz, Germany*

Sriram Sundaresan − *Department Chemie, Johannes Gutenberg-Universität Mainz, 55128 Mainz, Germany; Institute of Physics, Czech Academy of Sciences, 162 00 Prague, Czech Republic;* orcid.org/0000-0002-5753-8130

Luca M. Carrella − *Department Chemie, Johannes Gutenberg-Universität Mainz, 55128 Mainz, Germany;* orcid.org/0000-0001-9828-2912

Complete contact information is available at: https://pubs.acs.org/10.1021/acs.cgd.6c00054

Notes

The authors declare no competing financial interest.

ACKNOWLEDGMENTS

All the authors sincerely thank JGU Mainz for the funding and support. JGB and ER acknowledge funding by the Deutsche Forschungsgemeinschaft (DFG, German Research Foundation)-TRR 173-268565370 Spin+X (Project No. A04). Open Access funding enabled and organized by Projekt DEAL.

Instrument funding by the Deutsche Forschungsgemeinschaft (project no 518132540) is gratefully acknowledged.

REFERENCES

(1) Li, G.; Stefanczyk, O.; Kumar, K.; Guérin, L.; Okuzono, K.; Tran, K.; Seydi Kilic, M.; Nakabayashi, K.; Imoto, K.; Namai, A.; Nakamura, Y.; Ranjan Maity, S.; Renz, F.; Chastanet, G.; Ohkoshi, S. Near-Infrared Light-Induced Spin-State Switching Based on Fe(II)−Hg(II) Spin-Crossover Network. *Angew. Chem., Int. Ed.* **2025**, *64* (12), No. e202423095.

(2) Lünser, K.; Kavak, E.; Gürpinar, K.; Emre, B.; Atakol, O.; Stern-Taulats, E.; Porta, M.; Planes, A.; Lloveras, P.; Tamarit, J.-L.; Mañosa, L. Elastocaloric, Barocaloric and Magnetocaloric Effects in Spin Crossover Polymer Composite Films. *Nat. Commun.* **2024**, *15* (1), No. 6171.

(3) Dürrmann, A.; Hörner, G.; Baabe, D.; Heinemann, F. W.; De Melo, M. A. C.; Weber, B. Cooperative Spin Crossover Leading to Bistable and Multi-Inert System States in an Iron(III) Complex. *Nat. Commun.* **2024**, *15* (1), No. 7321.

(4) Charytanowicz, T.; Wang, J.; Tokoro, H.; Tran, K.; Renz, F.; Ohkoshi, S.; Chorazy, S.; Sieklucka, B. Thermal Bistability of Magnetic Susceptibility, Light Absorption, Second Harmonic Generation, and Dielectric Properties in a Polar Spin-Crossover Iron−Rhenium Chain Material. *Angew. Chem., Int. Ed.* **2025**, *64* (7), No. e202419242.

(5) Woo, K. S.; Zhang, A.; Arabelo, A.; Brown, T. D.; Park, M.; Talin, A. A.; Fuller, E. J.; Bisht, R. S.; Qian, X.; Arroyave, R.; Ramanathan, S.; Thomas, L.; Williams, R. S.; Kumar, S. True Random Number Generation Using the Spin Crossover in LaCoO3. *Nat. Commun.* **2024**, *15* (1), No. 4656.

(6) Fiaz, F.; Siddique, A.; Rabbee, M. F.; Hanif, M. B.; Al-Baqami, S. M.; Jillani, S. M. S.; Almuqati, N. S.; Rahman, Md. R.; Chowdhury, M. A.; Akhtar, M. N.; Khan, M. M. R.; Rahman, M. M.; Sheikh, T. A. Advances in Spin Crossover Metal Complexes: A Comprehensive Review on Its Gas Sensing Applications. *Rev. Inorg. Chem.* **2026**, *46*, 35−59.

(7) Zhang, Y.; Torres-Cavanillas, R.; Yan, X.; Zeng, Y.; Jiang, M.; Clemente-León, M.; Coronado, E.; Shi, S. Spin Crossover Iron Complexes with Spin Transition near Room Temperature Based on Nitrogen Ligands Containing Aromatic Rings: From Molecular Design to Functional Devices. *Chem. Soc. Rev.* **2024**, *53* (17), 8764−8789.

(8) Zhang, Y.; Rotaru, A.; Ranquet, T.; Yang, X.; Zan, Y.; Reig, B.; Séguy, I.; Salmon, L.; Molnár, G.; Bousseksou, A. Stress-Coupled Spin State Switching in a Spin Crossover Composite Modulates Current in an Organic Semiconductor. *J. Mater. Chem. C* **2025**, *13* (36), 18905−18912.

(9) Becker, J.-G.; Sundaresan, S.; Carrella, L. M.; Rentschler, E. Chirality without Compromise: Identical Spin Crossover Behavior between the Racemate and the Enantiopure Fe(II) Complexes. *Chem. Commun.* **2025**, *61*, 13389−13392, DOI: 10.1039/D5CC03779D.

(10) Ma, T.-T.; Sun, X.-P.; Yao, Z.-S.; Tao, J. Homochiral *versus* Racemic Polymorphs of Spin-Crossover Iron(II) Complexes with Reversible LIESST Effect. *Inorg. Chem. Front.* **2020**, *7* (5), 1196−1204.

(11) Mahbub, R.; McElveen, K. A.; Zaz, M. Z.; Ekanayaka, T. K.; Mishra, E.; Bissell, E.; Banerjee, P.; Shapiro, D.; Lai, R. Y.; Dowben, P. A.; Shield, J. E. Effect of Different Crystallographic Properties on the Electrical Conductivity of Two Polymorphs of a Spin Crossover Complex. *J. Phys.: Condens. Matter* **2025**, *37* (8), No. 085302.

(12) Kiehl, J.; Hochdörffer, T.; Carrella, L. M.; Schünemann, V.; Nygaard, M. H.; Overgaard, J.; Rentschler, E. Pronounced Magnetic Bistability in Highly Cooperative Mononuclear $[Fe(L^{npdtz})_2(NCX)_2]$ Complexes. *Inorg. Chem.* **2022**, *61* (7), 3141−3151.

(13) Petrenko, Y. P.; Troya, J.; García-López, V.; Khomenko, D. M.; Doroshchuk, R. O.; Lampeka, R. D.; Clemente-León, M.; Coronado, E. Stepwise Spin Transitions of Spin-Crossover Complexes Based in 3-(2-Pyridyl)-1,2,4-Triazole Ligands Associated with Symmetry Change in Hydrogen Bonding Interactions. *Inorg. Chem.* **2025**, *64* (13), 6442−6451.

(14) Dabb, S. L.; Fletcher, N. C. Mer and Fac Isomerism in Tris Chelate Diimine Metal Complexes. *Dalton Trans.* **2015**, *44* (10), 4406−4422.

(15) Morozumi, T.; Matsuoka, R.; Nakamura, T.; Nabeshima, T. Solvent-Dependent *Fac*/*Mer* -Isomerization and Self-Assembly of Triply Helical Complexes Bearing a Pivot Part. *Chem. Sci.* **2021**, *12* (22), 7720−7726.

(16) Zhao, X.-H.; Deng, Y.-F.; Huang, J.-Q.; Liu, M.; Zhang, Y.-Z. Solvated/Desolvated Homochiral Fe(II) Complexes Showing Distinct Bidirectional Photo-Switching Due to a Hidden State. *Inorg. Chem. Front.* **2024**, *11* (3), 808−816.

(17) Sundaresan, S.; Becker, J.-G.; Eppelsheimer, J.; Sedykh, A. E.; Carrella, L. M.; Müller-Buschbaum, K.; Rentschler, E. Synergetic Spin Singlet−Quintet Switching and Luminescence in Mononuclear Fe(II) 1,3,4-Oxadiazole Tetradentate Chelates with $NCBH_3$ Co-Ligand. *Dalton Trans.* **2023**, *52* (37), 13181−13189.

(18) Cuza, E.; Benmansour, S.; Cosquer, N.; Conan, F.; Pillet, S.; Gómez-García, C. J.; Triki, S. Spin Cross-Over (SCO) Anionic Fe(II) Complexes Based on the Tripodal Ligand Tris(2-Pyridyl)-Ethoxymethane. *Magnetochemistry* **2020**, *6* (2), No. 26.

(19) Zhou, J.; Zhu, B.-W.; Luan, J.; Liu, Z.; Fang, J.-K.; Bao, X.; Peng, G.; Tucek, J.; Bao, S.-S.; Zheng, L.-M. In Air a Spin Crossover Active Iron(II) Complex of Amine/$NCBH_3^-$ Ligands Is Converted to a Low Spin Complex of Imine/CN^- Ligands. *Dalton Trans.* **2015**, *44* (47), 20551−20561.

(20) Becker, J.-G.; Nüsing, J. F.; Sundaresan, S.; Diego, R.; Mondeshki, M.; Carrella, L. M.; Rentschler, E. Crucial Role of the Heteroatom and Bite Angle Influencing Spin States and Dinuclear Fe(II) Helicate Formation in 1,3,4-Thia/Oxadiazole Ligand. *Cryst. Growth Des.* **2024**, *24* (18), 7662−7669.

(21) Kisslinger, S.; Kelm, H.; Zheng, S.; Beitat, A.; Würtele, C.; Wortmann, R.; Bonnet, S.; Herres-Pawlis, S.; Krüger, H.; Schindler, S. Synthesis and Characterization of Iron(II) Thiocyanate Complexes with Derivatives of the Tris(Pyridine-2-ylmethyl)Amine (Tmpa) Ligand. *Z. Anorg. Allg. Chem.* **2012**, *638* (12−13), 2069−2077.

(22) Matouzenko, G. S.; Luneau, D.; Molnár, G.; Ould-Moussa, N.; Zein, S.; Borshch, S. A.; Bousseksou, A.; Averseng, F. A Two-Step Spin Transition and Order−Disorder Phenomena in the Mononuclear Compound $[Fe(Hpy\text{-}DAPP)](BF_4)_2$. *Eur. J. Inorg. Chem.* **2006**, *2006* (13), 2671−2682.

(23) Matouzenko, G. S.; Jeanneau, E.; Yu Verat, A.; Bousseksou, A. Spin Crossover and Polymorphism in a Family of 1,2-Bis(4-Pyridyl)Ethene-Bridged Binuclear Iron(Ii) Complexes. A Key Role of Structural Distortions. *Dalton Trans.* **2011**, *40* (37), 9608−9618.

(24) Sundaresan, S.; Eppelsheimer, J.; Gera, E.; Wiener, L.; Carrella, L. M.; Vignesh, K. R.; Rentschler, E. A Combined Theoretical and Experimental Approach to Determine the Right Choice of Co-Ligand to Impart Spin Crossover in Fe(II) Complexes Based on 1,3,4-Oxadiazole Ligands. *Dalton Trans.* **2024**, *53* (24), 10303−10317.

(25) Becker, J.-G.; Sundaresan, S.; Hochdörffer, T.; Wolny, J. A.; Carrella, L. M.; Schünemann, V.; Rentschler, E. Sub Lattice Driven Spin State Ordering and Coordination Elasticity in Fe(II) 1,3,4-Thiadiazole Complexes. *Dalton Trans.* **2026**, *55* (7), 2833−2844.

(26) Halcrow, M. A. Structure:Function Relationships in Molecular Spin-Crossover Complexes. *Chem. Soc. Rev.* **2011**, *40* (7), 4119−4142.

(27) Yuan, S.; Natt, N.; Powell, B. J. Impact of Molecular Distortions on Bistability in Spin Crossover Complexes. *Inorg. Chem.* **2025**, *64* (14), 7182−7193.

(28) Halcrow, M. A.; Berdiell, I. C.; Pask, C. M.; Kulmaczewski, R. Relationship between the Molecular Structure and Switching Temperature in a Library of Spin-Crossover Molecular Materials. *Inorg. Chem.* **2019**, *58* (15), 9811−9821.

(29) Feltham, H. L. C.; Johnson, C.; Elliott, A. B. S.; Gordon, K. C.; Albrecht, M.; Brooker, S. "Tail" Tuning of Iron(II) Spin Crossover Temperature by 100 K. *Inorg. Chem.* **2015**, *54* (6), 2902−2909.

(30) Rodríguez-Jiménez, S.; Barltrop, A. S.; White, N. G.; Feltham, H. L. C.; Brooker, S. Solvent Polarity Predictably Tunes Spin Crossover $T_{1/2}$ in Isomeric Iron(II) Pyrimidine Triazoles. *Inorg. Chem.* **2018**, *57* (11), 6266−6282.
(31) Furusho, D.; Nishi, K.; Hashibe, T.; Fujinami, T.; Hagiwara, H.; Matsumoto, N.; Halcrow, M. A.; Iijima, S.; Sunatsuki, Y.; Kojima, M. Assembly Structures and Spin Crossover Properties of Facial and Meridional Isomers of Tris[Benzyl(2-Methylimidazol-4-Ylmethylidene)Amine]Iron(II) Chloride Hexafluorophosphate. *Chem. Lett.* **2011**, *40* (1), 72−74.
(32) Furushou, D.; Hashibe, T.; Fujinami, T.; Nishi, K.; Hagiwara, H.; Matsumoto, N.; Sunatsuki, Y.; Kojima, M.; Iijima, S. Facial and Meridional Geometrical Isomers of Tris(2-Methylimidazol-4-Yl-Methylideneaminobenzyl)Iron(II) with Δ- and Λ-Configurations and Their Enantio-Discriminative Assembly via Imidazole···chloride Hydrogen Bonding and Spin Cross-over Properties. *Polyhedron* **2012**, *44* (1), 194−203.
(33) Banerjee, A.; Saha, A.; Saha, B. K. Understanding the Behavior of $\pi-\pi$ Interactions in Crystal Structures in Light of Geometry Corrected Statistical Analysis: Similarities and Differences with the Theoretical Models. *Cryst. Growth Des.* **2019**, *19* (4), 2245−2252.
(34) Zhao, X.; Deng, Y.; Xi, J.; Huang, J.; Zhang, Y. Supramolecular Spring-Like Fe(II) Spin-Crossover Complexes Experiencing Giant and Anisotropic Thermal Expansion Across Two Distinct Temperature Regimes. *Angew. Chem.* **2025**, *137* (8), No. e202414826.
(35) Gütlich, P.; Hauser, A.; Spiering, H. Thermal and Optical Switching of Iron(II) Complexes. *Angew. Chem., Int. Ed.* **1994**, *33* (20), 2024−2054.
(36) Habarakada, U.; Boonprab, T.; Harding, P.; Murray, K. S.; Phonsri, W.; Neville, S. M.; Ahmed, M.; Harding, D. J. Solvent Effects on the Structural and Magnetic Properties of Fe^{III} Spin-Crossover Complexes. *Cryst. Growth Des.* **2022**, *22* (8), 4895−4905.
(37) Fumanal, M.; Jiménez-Grávalos, F.; Ribas-Arino, J.; Vela, S. Lattice-Solvent Effects in the Spin-Crossover of an Fe(II)-Based Material. The Key Role of Intermolecular Interactions between Solvent Molecules. *Inorg. Chem.* **2017**, *56* (8), 4474−4483.
(38) Phonsri, W.; Harding, P.; Liu, L.; Telfer, S. G.; Murray, K. S.; Moubaraki, B.; Ross, T. M.; Jameson, G. N. L.; Harding, D. J. Solvent Modified Spin Crossover in an Iron(III) Complex: Phase Changes and an Exceptionally Wide Hysteresis. *Chem. Sci.* **2017**, *8* (5), 3949−3959.
(39) Schmid, R. Re-Interpretation of the Solvent Dielectric Constant in Coordination Chemical Terms. *J. Sol. Chem.* **1983**, *12* (2), 135−152.
(40) Armarego, W. L. F. *Purification of Laboratory Chemicals*; Butterworth-Heinemann: Amsterdam, 2017.
(41) Cobas, J. C.; Sardina, F. J. Nuclear Magnetic Resonance Data Processing. MestRe-C: A Software Package for Desktop Computers. *Concepts Magn. Reson.* **2003**, *19A* (2), 80−96.
(42) Sheldrick, G. M. *SHELXT* − Integrated Space-Group and Crystal-Structure Determination. *Acta Crystallogr. A Found. Adv.* **2015**, *71* (1), 3−8.
(43) Sheldrick, G. M. A Short History of *SHELX*. *Acta Crystallogr. A Found. Crystallogr.* **2008**, *64* (1), 112−122.
(44) Sheldrick, G. M.; Schneider, T. R. [16] SHELXL: High-Resolution Refinement. In *Methods Enzymology*; Elsevier, 1997; Vol. *277*, pp 319−343.
(45) Dolomanov, O. V.; Bourhis, L. J.; Gildea, R. J.; Howard, J. A. K.; Puschmann, H. *OLEX2*: A Complete Structure Solution, Refinement and Analysis Program. *J. Appl. Crystallogr.* **2009**, *42* (2), 339−341.
(46) Sundaresan, S.; Kiehl, J.; Carrella, L. M.; Rentschler, E. Effect of Methoxy Ligand-Substituent and NCE Coligands in Tuning $T_{1/2}$ of Coordinatively Elastic Fe(II) Spin Crossover Complexes. *Cryst. Growth Des.* **2023**, *23* (3), 1648−1655.
(47) Levadala, S. K.; Banerjee, S. R.; Maresca, K. P.; Babich, J. W.; Zubieta, J. Direct Reductive Alkylation of Amino Acids: Synthesis of Bifunctional Chelates for Nuclear Imaging. *Synthesis* **2004**, *11*, 1759−1766.
(48) Plaza-Lozano, D.; Ramírez-Palma, D.; Vela, A.; Olguín, J. High Spin Iron(II) Complexes Based on Imidazolyl- and 1,2,3-Triazolyl-Thione Ligands and NCE (E = S, Se or BH_3) Co-Ligands: Effect of the S-Functional Group on the Structural and Magnetic Properties. *New J. Chem.* **2022**, *46* (31), 14910−14921.

https://doi.org/10.1021/acs.cgd.6c00054
Cryst. Growth Des. 2026, 26, 4124−4132